Journal Pre-proof

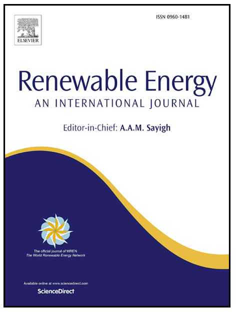

Performance assessment of a tidal turbine using two flow references

Magnus Harrold, Pablo Ouro, Tim O'Doherty

PII: S0960-1481(19)31924-X

DOI: https://doi.org/10.1016/j.renene.2019.12.052

Reference: RENE 12761

To appear in: *Renewable Energy*

Received Date: 16 May 2019

Revised Date: 15 November 2019

Accepted Date: 10 December 2019

Please cite this article as: Harrold M, Ouro P, O'Doherty T, Performance assessment of a tidal turbine using two flow references, *Renewable Energy* (2020), doi: https://doi.org/10.1016/j.renene.2019.12.052.

Magnus Harrold: Conceptualisation, Methodology, Formal analysis, Writing – Original Draft, Visualisation. **Pablo Ouro**: Formal analysis, Writing – Original Draft. **Tim O'Doherty**: Writing – Review & Editing.

Performance assessment of a tidal turbine using two flow references

Magnus Harrold[a,*], Pablo Ouro[b], Tim O'Doherty[b]

[a] *The University of Exeter, College of Engineering, Mathematics and Physical Sciences, Penryn, Cornwall, UK;*
[b] *Cardiff University, School of Engineering, Cardiff, UK;*

Abstract

The measurement of power performance is an important procedure in the design verification and ongoing health monitoring of a tidal turbine. Standardised methods state that the performance should be measured relative to two independently located flow sensors, the arrangement of which is often non-trivial and necessitates additional cost. Recent interest in the usage of flow sensors mounted on the turbine has demonstrated their capabilities in profiling the rotor approach flow, but this instrument configuration is not recognised in the performance assessment standard. This study evaluates the merits of the turbine mounted configuration by measuring the performance of a tidal turbine relative to this reference and to a conventional seabed placed instrument. The turbine mounted sensor is found to provide a better reference of the free-stream conditions, evident from an improved agreement with theoretical predictions of device performance and a reduced amount of variation in the results. This new method could reduce both the costs and uncertainty associated with existing performance assessment best practices.

Keywords: acoustic Doppler profiler, performance assessment, power curve, tidal energy, tidal turbine

*Corresponding author
Email address: `m.j.harrold@exeter.ac.uk` (Magnus Harrold)

1. Introduction

The power performance assessment of a tidal turbine is a means of relating the inflow current conditions to the output power of the device, leading to the development of a measured power curve. Typically this procedure is undertaken as a key step in the process of achieving type certification of the turbine [1], providing a basis to guarantee the power performance of the device to interested parties, e.g. customers, investors and insurers. Another reason for measuring the power curve is to validate the tools used by turbine designers. Only a few studies have compared theoretical predictions of tidal turbine performance with full-scale measurements, e.g. [2, 3], although there are several scale-model studies on this subject [4, 5]. In addition to design verification, ongoing monitoring of the turbine performance allows operators to assess the condition of the device [6], helping to identify if a fault has occurred and plan a maintenance intervention before a serious failure develops.

The SeaGen project commissioned in 2008 provided one of the first insights on the operational performance of a full-scale tidal turbine [7]. While it was reported that overall system efficiencies were in the region of 40 – 45%, one of the more interesting findings revealed that the turbine performed slightly better during ebb flows, believed to be due to flow enhancements from an upstream cross-beam on this tide. The SeaGen performance was evaluated against guidelines published by the European Marine Energy Centre (EMEC) [8]. These guidelines provided a methodology to ensure consistency in the measurement of power performance of tidal turbines, and were subsequently used as the basis for the first international technical specification, the IEC 62600-200 [9], published in 2013. The guidelines define where flow and power sensors should be placed, the minimum data capture requirements and a data processing method to derive a measured turbine power curve.

The IEC 62600-200 has since been used in a number of studies, arguably most extensively during the testing of a 1 MW turbine at EMEC [3], in which several flow sensors were used to measure performance. The results suggested that the location of these sensors did not have a significant effect on measured performance, even in the cases where sensors were located just outside of the recommended deployment areas in IEC 62600-200. Similarly, the work in [10] showed how the methodology could be applied to a tidal turbine mounted off a barge, highlighting that the time-varying power output could be as much as 50% greater than the time-averaged value due to site turbulence. Furthermore, in [11] the guidelines were used for a turbine deployment off the French coastline, although with some deviations from the technical specification. This included the absence of a flow sensor to measure the tidal current conditions, with these instead derived from a calibrated numerical model of the area. This led to quite a significant variation in performance between ebb and flood conditions that was not a true reflection of the device's capabilities, highlighting the importance of obtaining in situ measurements.

As a consequence of the IEC 62600-200 being published before many of the recent advances in the tidal energy sector, its application presents a number of challenges to suit all of the devices that have since emerged. For example, there are quite strict guidelines on the locations of flow sensors, with their placement being a function of the turbine equivalent diameter. This includes the preferred 'in-line orientation' which requires the sensor to be placed between $2-5$ equivalent diameters upstream of the turbine, and within $1/2$ an equivalent diameter of the rotor centreline laterally [9]. From a practical perspective, this becomes more challenging for turbines with smaller rotor diameters, e.g. the device in [10] would require the flow sensor to be installed within a 4 m lateral range. This is further complicated if the turbine is on a floating platform that is subject to surge and/or sway, with these motions effectively reducing the size of the acceptable area in which the flow sensor can be placed.

At present the IEC 62600-200 also does not recognise forward-looking flow sensors which profile in the horizontal plane, which can be installed on the turbine itself. This arrangement, therefore, does not require any additional costly offshore work to deploy flow sensors on the seabed. Increasingly turbine mounted flow sensors have been used in recent work, e.g. [3, 12, 13], in order to obtain a unique insight on the rotor approach flow. This paper aims to highlight some of the advantages of using these sensors for the purpose of power performance assessment, by comparing the operational measurements from a full-scale tidal turbine relative to both a turbine mounted and conventional seabed placed instrument. The paper is structured as follows: Section 2 provides an overview of the tidal turbine, its installation site and the key sensors relevant to this study; Section 3 details the analysis procedures used in the performance assessment; Section 4 reports on the key results obtained; Section 5 discusses these key findings in the context of existing best practices and outlines various advantages/disadvantages of using turbine mounted flow sensors; while Section 6 summarises this work to form a conclusion.

2. Test overview

2.1. Turbine description

The tested turbine is a 400 kW rated machine with a 3-bladed, 12 m diameter, fixed-pitch, horizontal-axis rotor, as shown in Figure 1. Behind the rotor the turbine nacelle hosts the drivetrain, which consists of a gearbox and induction generator. Device power is exported via a 6.6 kV subsea cable to shore, where the power conditioning is performed before being sent to the local distribution network. A hydraulic based yaw system with push rods allows the frame supporting the nacelle to rotate and face the changing tidal current direction, or park out of the flow during non-operational conditions. The hub centre is 12.1 m above the seabed, with the nacelle sitting atop an open tower, which itself is placed on one apex of a triangular based gravity frame.

The turbine was designed to follow a conventional variable speed control scheme, tracking the Tip-Speed-Ratio, λ, that corresponds to the point of maximum rotor power efficiency, $\lambda_{opt.}$, until reaching the rated power output of the generator (400 kW). This was predicted to occur in flow speeds of 2.7 m$\cdot s^{-1}$, once the losses in the turbine drivetrain were accounted for. The key turbine

Figure 1: 400 kW tidal turbine

parameters λ, generator power, $P_{gen.}$ and blade root bending moment, M_y, can be described as follows:

$$\lambda = \frac{\Omega \cdot r}{U_0} \tag{1}$$

$$P_{gen.} = \frac{1}{2} \cdot c_p(\lambda) \cdot \eta_{gbox.} \cdot \eta_{gen.} \cdot \rho \cdot \pi \cdot r^2 \cdot U_0^3 \tag{2}$$

$$M_y = \frac{1}{2} \cdot c_{M_y}(\lambda) \cdot \rho \cdot \pi \cdot r^3 \cdot U_0^2 \tag{3}$$

where Ω and r are the rotational speed and radius of the rotor, U_0 is the free-stream velocity, $c_p(\lambda)$ and $c_{M_y}(\lambda)$ are the rotor power and blade root bending moment coefficients respectively and both vary as a function of λ, $\eta_{gbox.}$ and $\eta_{gen.}$ are the efficiencies of the gearbox and generator respectively, and ρ is the water density.

After reaching its rated output, the generator power in higher flow conditions is held constant by allowing the rotor to overspeed to a higher λ, i.e. $\lambda > \lambda_{opt.}$, enabled through a reduction in generator torque. This power regulation philosophy differs from standard fixed-pitch control schemes, whereby the rotor is

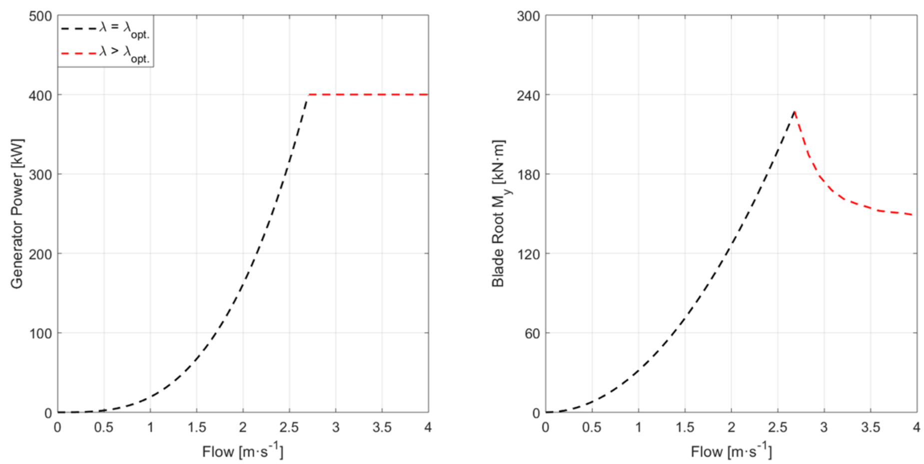

Figure 2: Turbine principles of operation regarding (a) generator power (kW) and (b) blade root bending moment, M_y (kN·m)

stalled in high flows. Stall based turbines have been shown to underperform relative to variable pitch turbines [14] and place greater torque demands on the generator to slow the rotor, which takes the device into a region of lower electrical efficiency (higher Joule losses). The overspeed control philosophy employed by the turbine considered in this work overcomes these shortcomings by reducing the torque demanded in above rated conditions, shifting the generator to a region of increased electrical efficiency and achieving a power performance at least equivalent to that of a variable pitch machine. The key advantage here being that the pitch system is not required to achieve this performance, reducing the number of sub-systems and potential failure modes. However, drawbacks of the overspeed control scheme include an increased risk of fatigue damage and cavitation. This was largely overcome by designing the rotor to operate within a low λ range with axial load reduction characteristics in the overspeed region. Figure 2 shows the principles of operation of the overspeed control strategy, the merits of which have been previously highlighted in a number of experimental [15, 16] and numerical [17, 4] studies, while interest in similar control philosophies has also been reported elsewhere [18, 19].

2.2. Deployment site conditions

The turbine was installed in 2015 at Ramsey Sound, a sea channel located off the south west coast of Wales, UK. The channel narrows between the Welsh mainland and Ramsey Island, creating energetic tidal currents that flow northwards through the site during flood tides, and southwards during ebb tides. Ramsey Island also provides good shelter from Atlantic waves in the tidal channel, reducing the likelihood of potentially damaging sources of cyclical loading on the turbine and increasing the likelihood of suitable weather windows to perform marine operations.

The directionality and strength of typical spring tidal currents at the turbine location are shown in Figure 3, as reported previously in [16]. The currents at the site are predominantly bidirectional, heading just $7 - 8^o$ from North/South. The flood tide, however, is considerably stronger at this location, reaching mean flows up to 2.8 $\text{m}\cdot\text{s}^{-1}$. This is due to the channel contracting both vertically and laterally upstream of the turbine on flood tides, i.e. to the south, forcing the flow to accelerate. The flood tide is also much more turbulent due to the flow being disturbed by a number of features of the site bathymetry, which has been reported **on** by others [20, 21]. In contrast to this, peak spring ebb flows reach up to 1.8 $\text{m}\cdot\text{s}^{-1}$ at the turbine location.

For the performance assessment that follows, results obtained in ebb flows only are considered since the majority of the initial turbine testing took place in these conditions, and hence more data are available. These conditions were much more suitable to gain confidence in operating the device, before testing in the harsher flood tides. This does, however, mean that the reproduction of a power curve up to and above the rated point of the turbine is not possible, since the maximum ebb flows do not reach the rated 2.7 $\text{m}\cdot\ \text{s}^{-1}$.

The IEC 62600-200 recommends surveying the bathymetry at the turbine deployment site out to 5 equivalent diameters (D) either side of the turbine, and 10 D upstream and downstream, covering an area of 10 D $\times$ 20 D [9]. This region is shown in Figure 4, with the area offset by 8° to align with the dominant flood flow direction (see Figure 3). The turbine frame is depicted to

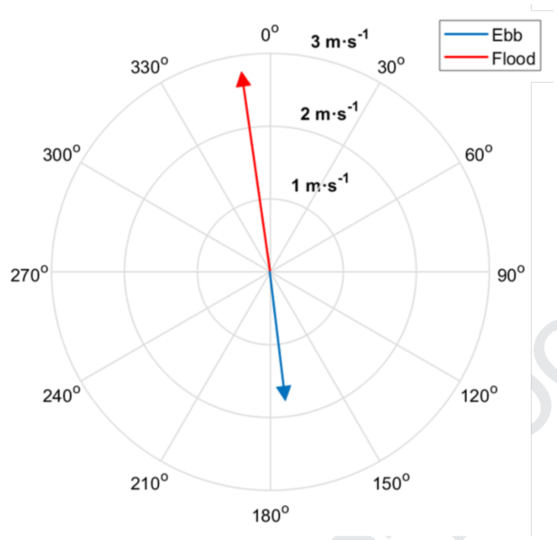

Figure 3: Typical directionality and strength of peak spring ebb and flood tides at Ramsey Sound

scale, with the rotor sitting atop the northernmost apex of the triangle. The frame was installed with a slight offset from dominant flow directions, but the yaw mechanism ensured that the rotor could be rotated to face both tides.

The site bathymetry, as shown in Figure 4, was surveyed on more than one occasion to pinpoint a suitable installation location for the turbine. A relatively flat ridge to the east of the northern portion of a trench that runs through Ramsey Sound was selected to accommodate the turbine frame, sited in a mean depth of 35 m. The depth within the 10 D $\times$ 20 D area ranges from 31 m at just over 5 D to the north of the turbine, to 44 m near the north-west corner of the area of interest. The latter is considered far enough away from the turbine, both longitudinally and laterally, to create any significant disturbance on the turbine flow, while the former is an elevation difference of just 4 m. In addition, Togneri et al. [21] reported elsewhere that the ebb tidal flow is not particularly turbulent at this location, especially when compared to the flood flow.

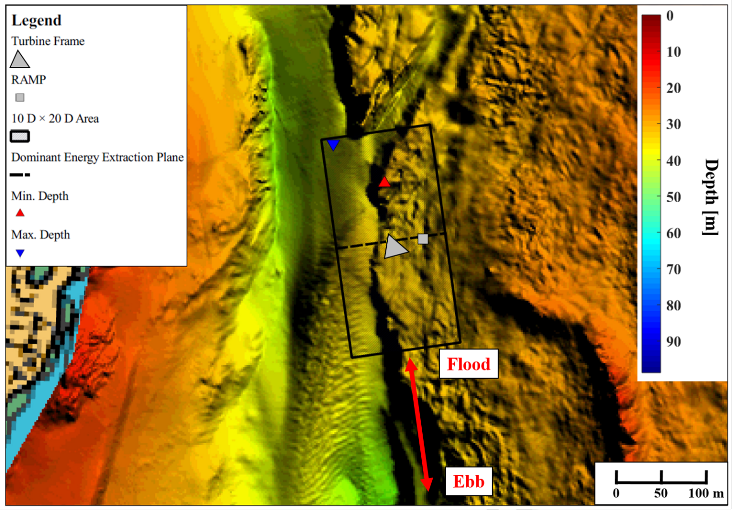

Figure 4: Bathymetry in the vicinity of the turbine, with the box showing the 10 D × 20 D area of interest

2.3. Instrumentation

The location of a small gravity structure referred to as the Remote Acoustic Monitoring Platform (RAMP) is also shown in Figure 4. The RAMP housed sensors for environmental monitoring, including an acoustic Doppler profiler to measure the flow conditions. The RAMP was installed 35 m to the east of the turbine and just 2 m below the dominant energy extraction plane, in a mean depth of 35 m. A short subsea cable between the RAMP and the turbine enabled the sensors to be powered and controlled from shore, preventing any limitations on battery life. Figure 5(a) shows the RAMP structure ahead of its installation.

The ADP within the RAMP, referred to as the seabed ADP, was a 600 kHz Teledyne RDI Workhorse Sentinel 4-beam instrument, with the beams oriented 20° **from vertical**. This instrument was capable of capturing the three-dimensional flow velocities from its location across the water column. The instrument was configured to sample at 1 Hz with a 0.75 m bin resolution, with the first measurement above the seabed at an elevation of 1.86 m.

A secondary ADP was placed in the centre of the turbine rotor, as shown in Figure 5(b). The turbine ADP was a 1 MHz Nortek Aquadopp instrument, fitted

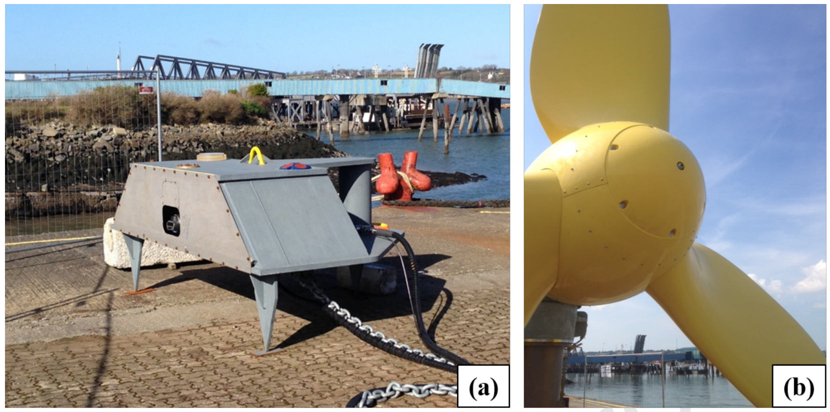

Figure 5: The RAMP structure housing the seabed ADP (a) and the turbine ADP visible in the rotor centre (b)

with a bespoke single-beam head piece with a narrow beam angle. By positioning the instrument in the rotor, the line-of-sight flow velocities (x-component) at the hub-height could be measured. The instrument was configured to sample at 1 Hz with a 1 m bin resolution, within a range of 1.4 - 20.4 m upstream of the turbine. This approach is not dissimilar to leading methods used to measure approaching wind velocities for wind turbines, in which turbine mounted LIDAR systems are used [22].

The turbine power measurements considered for the performance assessment were obtained at 1 Hz from the output of the generator, since this is a metric that can be used for a direct comparison with numerically predicted performance (Figure 2). An additional measurement was obtained onshore after the power was subject to losses as a result of transmission and conversion, while a further measurement was taken at the point of export to the grid. However, there are a number of assumptions required to estimate the losses encountered between the generator and these measurement points. The purpose here is to form the most reliable comparison with numerical performance, rather than strictly adhere to the IEC 62600-200 requirements, which states that the power should be measured at the output terminals of the device, i.e. the power exported to the grid after accounting for all losses, and in the form of the network electrical frequency.

The rotor blades were equipped with fibre-optic strain gauges to determine the forces acting on them. These measurements are used later in the paper as an additional means of evaluating the turbine performance characteristics relative to the two flow references. Specific details on these sensors and their capabilities can be found in Harrold and Ouro [16].

3. Performance assessment procedure

3.1. Seabed ADP

The seabed ADP did not meet the incident resource measurement requirements of the IEC 62600-200 for two reasons: firstly, two ADPs are required for the adjacent configuration (referred to as orientation B) with one placed either side of the turbine; secondly, the measurement volume of the ADPs should be within 1 - 2 equivalent diameters from the extent of the turbine rotor [9], or 18 - 30 m in this case. Figure 6 illustrates where these measurement volumes should have been taken, compared with where the ADP actually sampled. The reason for the ADP being located at this distance away from the turbine was to accommodate an active sonar system in the RAMP, which needed at least this range to have sufficient vertical coverage of the rotor. Meanwhile, just one ADP was used to minimise the costs associated with an additional seabed deployment. In tidal environments subject to considerable lateral velocity shear, using a sole ADP in this arrangement will inevitably have consequences on the suitability of the measurements as a turbine flow reference, leading to an inaccurate power curve. The recommended additional sensor can be used to reduce these effects by averaging the flow measurements between ADPs.

Despite the seabed ADP failing to meet the requirements of IEC 62600-200, the data processing guidelines from the document were still adhered to, specifically the **method of bins** [9]. To summarise this process, the power weighted flow magnitudes were firstly calculated by integrating the measurements obtained over the 17 ADP bins that sat at the elevations across the rotor plane.

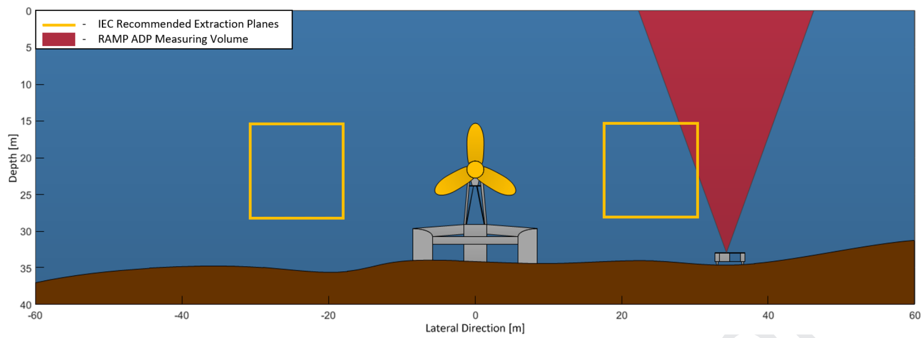

Figure 6: Planar view of the turbine along the dominant energy extraction plane

Greater weighting was given to measurements near the rotor centre elevation, while the least amount of weighting was applied to the lowermost and uppermost elevations. These spatially averaged measurements were then temporally averaged over 10-minute periods, before being sorted into bins at 0.1 m$\cdot$ s^{-1} intervals. The measurements that sit within each bin were then averaged further, reducing the data to a single point for each bin.

All of the seabed ADP 10-minute averaged flow magnitudes with respect to elevation, $U(z)$, across the rotor disk are shown in Figure 7, with all measurements normalised by the hub-height value, U_{Hub}. These are compared with the mean profile and a $1/7^{th}$ power law, which is typically used to describe the vertical variation in tidal current strength. However, it is observed here that the ebb tide at the site does not show a good agreement with this behaviour, with weaker and stronger currents found below and above the hub-height respectively. This suggests that a power law with a greater exponent would be more suitable, evident from the improved agreement shown with the $1/5^{th}$ power law also plotted in Figure 7.

3.2. Turbine ADP

Since there is no established methodology for processing the turbine ADP measurements, a procedure was developed after studying the inflow profiles obtained from the instrument. It was observed that at ranges greater than 1 $\times$ D, there is little variation in the longitudinal flow velocity, while a deceleration

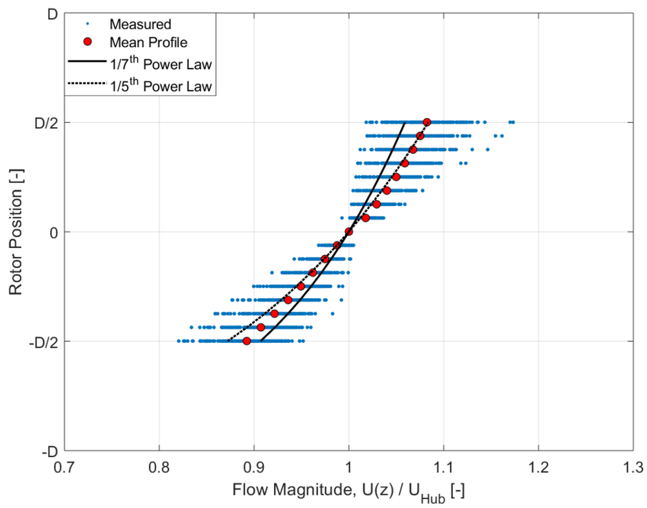

Figure 7: Flow magnitudes across the rotor disk, normalised by the hub-height value

occurs nearer the turbine as the flow field expands around the rotor. This is shown in Figure 8, where the 10-minute averaged longitudinal velocities, $u(x)$ are profiled with respect to upstream range, with all measurements normalised by the mean of the values obtained at ranges greater than $1 \times$ D. A mean profile from all of the measurements is also displayed, showing that typically there is less than a 1% variation in flow velocities obtained upstream of $1 \times$ D, although there are individual profiles at these ranges with scatter showing as high as 3% variation. However, at less than $0.5 \times$ D the flow velocities reduce to $\approx$ 0.83 of those obtained further upstream, while there is also a greater amount of variation between individual profiles [16]. As a result of the longitudinal velocities stabilising at ranges greater than $1 \times$ D, the mean of the values obtained at these ranges was considered the undisturbed longitudinal velocity reference, u_0, for the turbine mounted ADP. This also agrees with research by others [3] where it was observed that ranges less than $1 \times$ D were insufficient to obtain the free-stream conditions from a turbine mounted ADP.

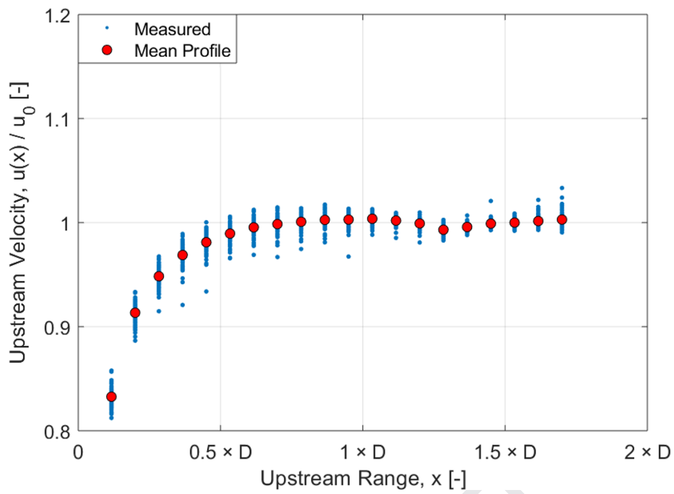

Figure 8: Longitudinal velocity as a function of upstream range, normalised by the free-stream value

3.3. *Turbine power*

During the test period the turbine was run using a preliminary controller not representative of its intended method of operation. Rather than operating in a variable-speed control scheme to track the maximum rotor efficiency at λ_{opt}, as described in [15], the turbine was run in a semi-fixed speed mode of operation. This involved the generator receiving commands to change rotor's rotational speed every minute, holding that speed constant until the next command. The commands were based on the mean hub-height flow speed obtained from the seabed ADP, with the rotor speed adjusted such that it operated at a tip speed corresponding to the point of maximum efficiency. This had consequences on the performance of the turbine for a number of reasons. Firstly, the seabed ADP was not upstream of the turbine and might not necessarily provide a good reference of the free-stream conditions, as discussed in Section 3.1. The flow information is also historical since it is obtained over the preceding 1-minute period, whereas the conditions could change significantly in the next 1-minute period. This also limits the update rate of the controller to the same period, again during which time the turbulent flow conditions can vary considerably.

Unfortunately, the designed variable-speed controller could not be implemented before the test campaign ended.

As shown later **in the paper** (Section 4), this sub-optimum controller resulted in considerable variation in device performance. For this reason, the data have been filtered to highlight periods where the turbine operated close to its intended design points, providing a more accurate representation of achievable performance. However, all data are still presented for completeness. The filtering method was based on the proximity of the generator RPM and torque data to the designed variable-speed curve. In order to track the optimum rotor efficiency, the generator torque demand, $\tau_{gen.}$ is calculated as follows:

$$\tau_{gen.} = k_\lambda \cdot \Omega^2_{gen.} \tag{4}$$

Where k_λ is a gain term determined by the desired λ and $\Omega_{gen.}$ is the generator speed. This relationship is represented by the dashed black line in Figure 9. It can be seen that most of the measurements are found to the right-hand-side of this curve, meaning that the rotor was generally overspeeding. There are, however, a number of points that lie within 10% of the desired curve. These are the data points that were processed separately to filter out any points that are clearly unrepresentative of device performance. It should also be noted that the generator data are 10-minute mean values, which means that even though there are points that on average lie close to the desired curve, these points could still consist of periods where the turbine was both over and underspeeding in excess of 10%. The consequences of the sub-optimum turbine controller on performance are discussed in more detail later in the paper.

3.4. Numerical modelling

The recorded power measurements are compared with those predicted using Tidal Bladed, a commercially available blade-element-momentum (BEM) based model [23, 2]. The power losses in the gearbox and generator were accounted for in the simulations using data provided by the component manufacturers. Both

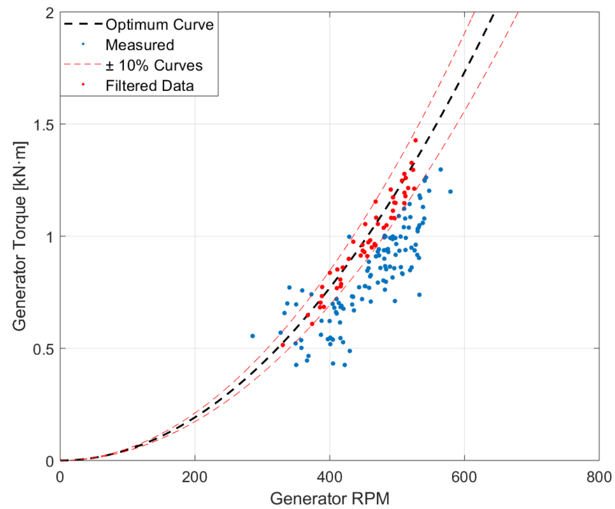

Figure 9: Filtered generator data (red scatter) that lie within 10% of the designed torque-speed curve (black dashed line)

steady and dynamic simulations were run, with the latter incorporating turbulence representative of the site based on data from a seabed ADP deployment prior to the turbine installation. This included a turbulence intensity of 15%, which is broadly in agreement with measurements obtained during turbine operation, as reported in [16]. The dynamic simulations were performed at mean hub flow speeds U_{hub} of 1, 1.5, 2, 2.5 and 3 m$\cdot$ s^{-1}, and repeated six times at each with a different turbulence seeding. Further details on these simulations are reported in [17].

4. Results

4.1. Free-stream conditions

The free-stream flow conditions from the two ADPs are compared in Figure 10, after processing as detailed in Section 3. While there is a clear correlation in the derived results and all data agree to within 15%, the seabed ADP consistently obtained stronger flows. This is not surprising given that the seabed ADP

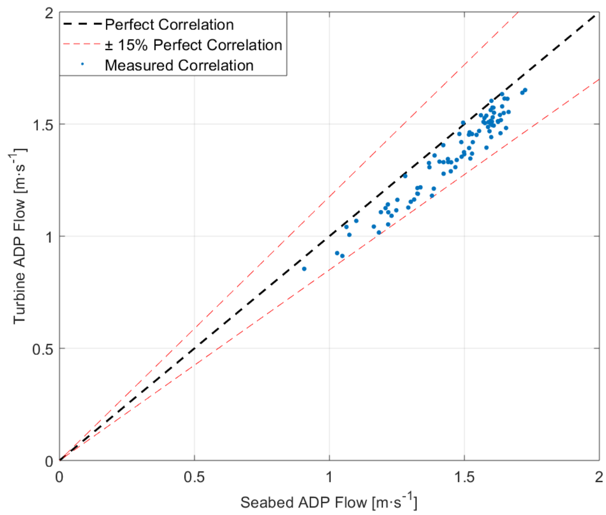

Figure 10: Correlation between the seabed and turbine ADP free-stream conditions

determines flow magnitude while the turbine ADP measures one component of the flow. These instrumentation differences should not have a significant effect on the results, since the majority of the flow magnitude is comprised of the longitudinal component obtained by the turbine ADP. It is possible that a slight bias could exist due to the differing spatial averaging methods used, which are vertical and horizontal averaging for the seabed and turbine ADPs respectively. However, this would again not be expected to account for some of the larger variations observed in the results. Instead, it is more likely that these are due to spatial variation at the turbine site, with the seabed ADP being placed at a location with stronger flows. In addition to this, any yaw misalignment will lead to the turbine ADP experiencing weaker flows. Some yaw corrections were applied manually during testing, but generally these were kept to a minimum by the turbine operator.

4.2. Power performance

All of the 10-minute average generator power measurements used in this performance assessment are shown in Figure 11, both relative to the seabed and turbine ADP flows. An additional data set has been produced to highlight the periods in which the turbine operated close to its intended design points, referred to as 'Optimum Periods' and as discussed previously in Section 3.3 (see Figure 9). The maximum and minimum values obtained within each 10-minute period are also shown, as is the steady-state power curve predicted by the numerical model.

The mean power measurements are generally found below the predicted curve, implying the device underperformed. This result should be expected given the sub-optimum control scheme used to run the turbine (see Section 3.3). However, it is evident that the turbine operated closer to the predicted curve in the filtered data set, suggesting that the device performance would be in better agreement with theory with the addition of the variable-speed controller.

In terms of the two flow references, a better agreement with the predicted curve is found using the turbine ADP. The variation in results is also much lower using this reference, evident from the narrower scatter. Some of the maximum values sit close to or lie below the predicted curve in the seabed ADP reference, meaning that the entire range of power measurements were low during such periods. This is surprising even after taking into consideration the sub-optimum turbine controller. It is more likely that these findings highlight that there are periods in which the seabed ADP does not provide a representative free-stream flow measurement.

Comparing the maximum values with those predicted in dynamic simulations at 1.0 and 1.5 $m \cdot s^{-1}$, the measured values are lower. This could be a consequence of the measured power being output as 1-second average values, whereas the numerical model time-step was much lower than this (0.05 seconds).

In order to complete the performance assessment, the mean power measurements were sorted into flow bins in increments of 0.1 $m \cdot s^{-1}$. The mean flow and power within each bin was then calculated. In accordance with 62600-200 [9], each bin comprises at least 30-minutes of data. Only the filtered data from Figure 11 were used to produce the finalised curves. The results relative to both flow references are shown in Figure 12. The seabed ADP results range

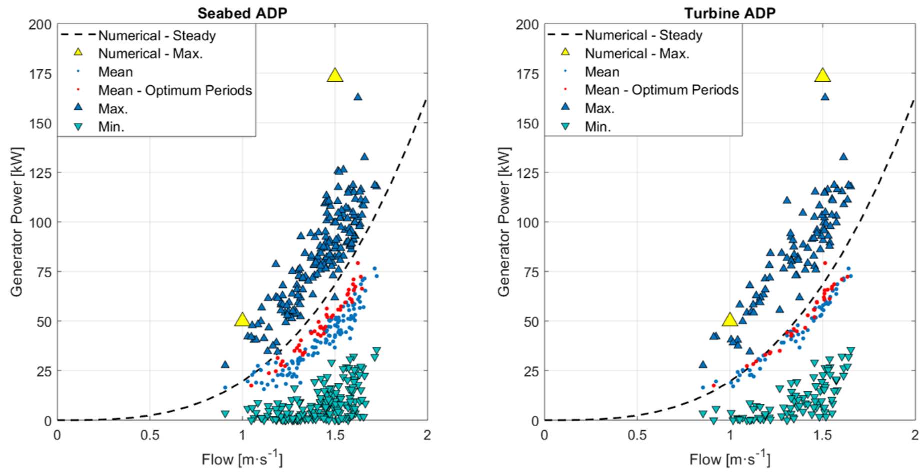

Figure 11: Dynamic power curves measured relative to the seabed (left) and turbine (right) ADPs

from 79 – 82% of the predicted values by the numerical model, while the turbine ADP results range from 86 – 102%. The latter provides evidence that the potential performance of the turbine is in-line with theory, but a variable-speed control strategy is required to achieve it. Meanwhile the lower than expected seabed ADP results cannot be explained solely by the turbine controller, with spatial variations in the flow and any yaw misalignment also contributing to underperformance.

4.3. Blade root bending moments

Comparing the measured blade root bending moments, M_y, with the numerical predictions provides further insight on the suitability of the flow references used. These are less susceptible to measurement uncertainties since the bending moments are proportional to the square of flow speed (Eqn. 3), whereas power is proportional to the cube (Eqn. 2). In addition to this, the λ which corresponds to the maximum c_p is not coincident with the peak in c_{M_y}, as shown in [16]. This means that the sub-optimum controller has a reduced influence on the expected loading characteristics, since the bending moments are predicted

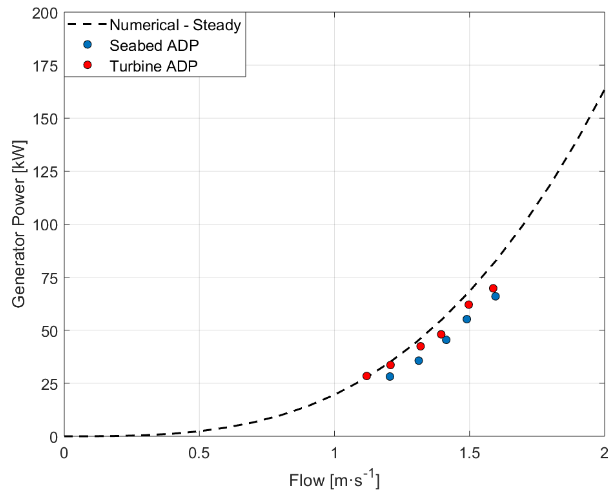

Figure 12: Turbine power curves measured relative to the seabed (blue) and turbine (green) ADPs

to decrease during overspeed and increase for slight underspeeds, whereas power decreases for both.

These hypotheses are supported by Figure 13, where it is observed that the 10-minute average bending moments are found to be in better agreement with theory than the power results (Figure 11). This is particularly true for the turbine ADP results, which scatter closely about the steady-state theoretical curve. As before, the seabed ADP results are subject to greater variation and the measurements show improved agreement when considering only the filtered periods. Generally the measured data are still found below the theoretical curves, due to the fact that the turbine was usually overspeeding (Figure 9) and hence operating at a tip-speed-ratio with a lower c_{M_y}. The maximum values are also found to show an improved agreement with theory, which is believed to be due to a combination of the higher sampling rate used for these measurements (16 Hz) and the aforementioned reasons.

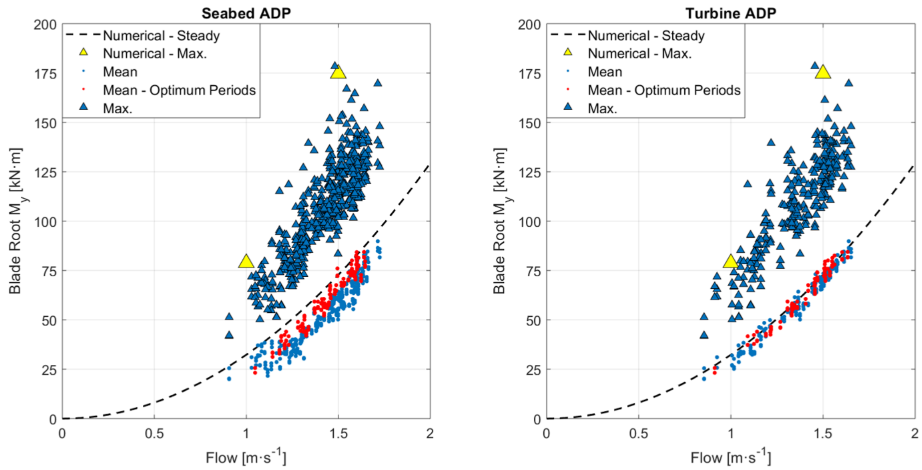

Figure 13: Dynamic blade root M_y curves measured relative to the seabed (left) and turbine (right) ADPs

5. Discussion

This paper has demonstrated how turbine performance metrics are sensitive to the flow reference used. Considering firstly the seabed ADP, there were clearly periods in which this reference was inadequate. This is not a fault of the instrument itself, but a consequence of the considerable lateral distance between the ADP and the turbine (Figure 6), leading to spatial differences in the flow. These results provide justification for the preference of ADPs to be placed upstream of the turbine in IEC 62600-200, or closer to and either side of the turbine in the adjacent configuration [9]. However, both of these configurations require two ADPs to be deployed to capture both the undisturbed ebb and flood conditions. Installing an ADP at the required position can be challenging at energetic tidal sites due to uneven bathymetries and the short time-frames in which marine operations must be undertaken, implying that to do this twice could be particularly onerous.

In contrast to this, turbine mounted ADPs do not require any additional deployments of seabed structures and the ebb and flood flows can be measured with just one instrument, provided that the turbine has a yaw mechanism. Due to the integration of the sensor with the turbine, the ADP can also be easily powered alongside other auxiliary equipment, preventing any limitations on battery life. This also enables communication with the instrument after deployment, allowing the transfer of data and the option to change configuration settings, e.g. sampling rate or spatial resolution. These are all limitations of remote ADP deployments, where considerable thought must be given to the effect that the instrument setup has on battery life and available memory storage. Furthermore, there is no means of restarting the remote instrument in the event of it crashing. The seabed ADP considered in this work was cabled to the turbine in order to avoid these limitations, but this is not always practical and requires additional expense.

In terms of the velocity measurements obtained from the turbine ADP, it was observed that free-stream conditions unaffected by the turbine presence were achieved at upstream ranges greater than 1 equivalent diameter. This is lower than the stated minimum range for upstream ADPs in IEC 62600-200, which recommends at least 2 equivalent diameters. The basis of this is thought to be practical in order to avoid subsea work in proximity to the turbine, but the evidence here suggests that this recommendation could be relaxed, at least for turbine ADPs. The ability to profile with respect to upstream range also allows any features that could negatively impact device performance to be identified. A separate analysis of the flood data from this test campaign highlighted that the rotor loading characteristics differed significantly from the ebb results, attributable to the turbine being positioned downstream of its base frame [16]. The turbine ADP measurements identified a reduction in the approach flow occurring at the same position as the frame extent. This disturbance would not have been observed with a seabed ADP deployment.

There are also several limitations of turbine ADPs. In this particular study, the turbine ADP was only capable of measuring one-component of the flow velocity since a single-beam instrument was used. As stated previously, this is not expected to have a significant effect on the derived results provided that the vertical velocity component, or z-component, is small. The two-dimensional magnitude is captured by the single-beam if the rotor is exactly perpendicular to the flow, since the lateral component, or y-component, would be equal to zero in the frame of reference of the instrument. If the rotor is misaligned with the flow, then the single-beam effectively accounts for the misalignment angle as it still measures the reduced velocity component perpendicular to the rotor. This could be useful for devices which are installed with a misalignment and do not have a yaw mechanism, providing a means of justifying achievable performance claims. Alternatively, the turbine could be equipped with a multi-beam ADP to obtain the three-dimensional flow. This would mean that the spatial averaging over the slanted beams would be performed vertically, providing an opportunity to average over the rotor elevation rather than that at just the hub-height. However, this would not be equivalent to the power weigthed rotor average in IEC 62600-200 [9]. It would also be necessary for the instrument to be fixed to prevent any measurement issues associated with rotating beams. This was not crucial for the hub-height single-beam instrument used in this study. To provide further insight on the relative strengths of instrument configurations, future work should aim to compare the measurements from a turbine ADP and an upstream positioned ADP. This would reduce the uncertainty associated with spatial variation encountered in this work.

Despite efforts to filter periods in which the turbine operated close to its intended design points, the device still underperformed relative to expectation. This highlights the importance of turbine control on device performance. Many scale-model studies implement simple fixed-speed control schemes to test turbines, but the results here have shown that this can lead to considerable variation in performance in a turbulent environment. The sub-optimum operation of the turbine complicated any evaluation of the suitability of the numerical model, even though the bending moment results, which were less susceptible to the controller, showed good agreement, both in terms of the mean and maximum values. Further validation should be reserved for cases in which the same controller is used, with particular attention given to the non-standard blade element momentum features added to tidal turbine models, e.g. added mass and buoyancy effects.

6. Conclusions

The performance characteristics of a full-scale tidal turbine have been measured relative to two flow speed references, an adjacently deployed seabed ADP and a rotor mounted turbine ADP, with the assessment adhering to the guidelines of the IEC 62600-200 [9] where possible. Power measurements were compared to theoretical predictions of device performance. It was found that there are periods in which the seabed ADP does not provide a good reference of the free-stream conditions experienced by the turbine, evident from the lower than expected performance measurements and the greater amount of scatter in results. Some of these findings can be attributed to the turbine running a sub-optimum control scheme during the test campaign. Despite this, the turbine ADP results were found to be closer to the theoretical predictions of device performance and were subject to less variation, implying that it provided a better reference of the flow conditions. These results are encouraging considering that turbine ADP configurations are currently not recognised in IEC 62600-200, despite offering several practical advantages and cost savings. Future work should explore the comparison of performance relative to a turbine ADP and an upstream positioned seabed ADP, the latter of which is the preferred deployment location for these instruments.

Acknowledgements

M.H. wishes to acknowledge the support received from the Industrial Doctoral Centre for Offshore Renewable Energy (IDCORE) programme that enabled the initial analysis of the reported data. IDCORE is funded by the Energy Technologies Institute (ETI) and the EPSRC RCUK Energy programme.

References

[1] DNV GL, DNVGL-SE-0163 - Certification of tidal turbines and arrays, Tech. rep., DNV GL AS (2015).

[2] S. Parkinson, W. Collier, Model validation of hydrodynamic loads and performance of a full-scale tidal turbine using Tidal Bladed, International Journal of Marine Energy 16 (2016) 279–297.

[3] J. McNaughton, R. Sinclair, B. Sellar, Measuring and modelling the power curve of a commercial-scale tidal turbine, in: Proceedings of the 11^{th} European Wave and Tidal Energy Conference (EWTEC), Nantes, France, 2015.

[4] P. Ouro, M. Harrold, T. Stoesser, P. Bromley, Hydrodynamic loadings on a horizontal axis tidal turbine prototype, Journal of Fluids and Structures 71 (2017) 78–95. doi:10.1016/j.jfluidstructs.2017.03.009.

[5] A. Mason-Jones, D. O'Doherty, C. Morris, T. O'Doherty, C. Byrne, P. Prickett, R. Grosvenor, I. Owen, S. Tedds, R. Poole, Non-dimensional scaling of tidal stream turbines, Energy 44 (1) (2012) 820–829.

[6] Z. Hameed, Y. Hong, S. Ahn, C. Song, Condition monitoring and fault detection of wind turbines and related algorithms: A review, Renewable and Sustainable Energy Reviews 13 (1) (2009) 1–39.

[7] P. Fraenkel, Development and testing of marine current turbine's seagen 1.2 mw tidal stream turbine, in: Proceedings of the 3^{rd} International Conference on Ocean Energy (ICOE), Bilbao, Spain, 2010.

[8] The European Marine Energy Centre (EMEC), Assessment of performance of tidal energy conversion systems, Tech. rep., EMEC (2009).

[9] International Electrotechnical Commission (IEC), IEC/TS 62600-200. Marine energy - Wave, tidal and other water current converters - Part 200: Electricity producing tidal energy converters - Power performance assessment, Tech. rep., International Electrotechnical Commission (IEC) (2013).

[10] P. Jeffcoate, R. Starzmann, B. Elsaesser, S. Scholl, S. Bischoff, Field measurements of a full scale tidal turbine, International Journal of Marine Energy 12 (2015) 3–20. doi:https://doi.org/10.1016/j.ijome.2015.04.002.

[11] P. Fraenkel, Power performance assessment of the tidal turbine sabella d10 following iec62600-200, in: Proceedings of the ASME 35^{th} International Conference on Ocean, Offshore and Arctic Engineering (OMAE), Busan, South Korea, 2016.

[12] M. Verbeek, R. Labeur, W. Uijttewaal, P. de Haas, The near-wake of horizontal axis tidal turbines in a storm surge barrier, in: Proceedings of the 12^{th} European Wave and Tidal Energy Conference (EWTEC), Cork, Ireland, 2017.

[13] B. Sellar, G. Wakelam, D. Sutherland, D. Ingram, V. Venugopal, Characterisation of Tidal Flows at the European Marine Energy Centre in the Absence of Ocean Waves, Energies 11. doi:doi:10.3390/en11010176.

[14] B. Whitby, C. E. Ugalde-Loo, Performance of pitch and stall regulated tidal stream turbines, IEEE Transactions on Sustainable Energy 5 (1) (2014) 64–72. doi:10.1109/TSTE.2013.2272653.

[15] M. Harrold, P. Bromley, D. Clelland, M. Broudic, Demonstrating a tidal turbine control strategy at laboratory scale, in: Proceedings of the ASME 35^{th} International Conference on Ocean, Offshore and Arctic Engineering (OMAE), Busan, South Korea, 2016.

[16] M. Harrold, P. Ouro, Rotor loading characteristics of a full-scale tidal turbine, Energies 12 (6). doi:10.3390/en12061035.

[17] M. Harrold, P. Bromley, D. Clelland, A. Kiprakis, M. Abusara, Evaluating the thrust control capabilities of the deltastream^{TM} turbine, in: Proceedings of the 11^{th} European Wave and Tidal Energy Conference (EWTEC), Nantes, France, 2015.

[18] A. Winter, Speed regulated operation for tidal turbines with fixed pitch rotors, in: Proceedings of the MTS/IEEE OCEANS Conference, Kona, Hawai'i, USA, 2011.

[19] K. Gracie-Orr, T. Nevalainen, C. Johnstone, R. Murray, D. Doman, M. Pegg, Development and initial application of a blade design methodology for overspeed power-regulated tidal turbines, International Journal of Marine Energy 15 (2016) 140–155. doi:10.1016/j.ijome.2016.04.006.

[20] P. Evans, A. Mason-Jones, C. Wilson, C. Wooldridge, T. O'Doherty, D. O'Doherty, Constraints on extractable power from energetic tidal straits, Renewable Energy 81 (2015) 707–722.

[21] M. Togneri, I. Masters, Micrositing variability and mean flow scaling for marine turbulence in Ramsey Sound, Journal of Ocean Engineering and Marine Energy 2 (2016) 35–46.

[22] J. Trujillo, F. Bingol, G. Larsen, J. Mann, M. Kuhn, Light detection and ranging measurements of wake dynamics. Part II: two-dimensional scanning, Wind Energy 14 (2011) 61–75. doi:10.1002/we.402.

[23] Bossanyi, E., Tidal bladed theory manual, Tech. rep., DNV GL (2015).

- The power curve from a full-scale tidal turbine is measured
- Measurements from conventional seabed instrument inadequately capture turbine flows
- A new method is proposed using measurements obtained from a turbine mounted sensor
- Turbine sensor results show less variation and are in better agreement with theory
- New method reduces costs and uncertainties associated with performance assessment

Declaration of interests

☒ The authors declare that they have no known competing financial interests or personal relationships that could have appeared to influence the work reported in this paper.

☐The authors declare the following financial interests/personal relationships which may be considered as potential competing interests: